Journal of Advanced Marine Engineering and Technology, Vol. 49, No. 6, pp. 424~432, 2025
J. Advanced Marine Engineering and Technology (JAMET)
https://doi.org/10.5916/jamet.2025.49.6.424

ISSN 2234-7925 (Print)
ISSN 2765-4796 (Online)
Original Paper

Thermodynamic analysis of supercritical CO_2 power cycle for waste heat recovery of ammonia gas turbine

Jun-Seong Kim[1] · Do-Yeop Kim[2] · You-Taek Kim[†]

(Received November 10, 2025 ; Revised November 28, 2025 ; Accepted December 22, 2025)

Abstract: This study presents a thermodynamic analysis of a supercritical CO_2 (SCO_2) power cycle for waste heat recovery from an ammonia-fueled marine gas turbine. The ammonia gas turbine and SCO_2 power cycles were modeled, and the effects of key design variables were evaluated. Thermodynamic simulations were performed under steady-state conditions using a commercial process simulation program. Parametric analyses were conducted for ammonia inlet pressure, gas turbine inlet temperature, CO_2 turbine inlet pressure, minimum approach temperature of CO_2 heater, and cooling water outlet temperature of CO_2 cooler. The results indicate that higher ammonia inlet pressures and gas turbine inlet temperatures improve both the system efficiency and heat recovery rate. Reducing the minimum approach temperature in the CO_2 heater improves the cycle performance. Meanwhile, the CO_2 turbine inlet pressure and the cooling water outlet temperature of the CO_2 cooler have specific ranges that maximize the system efficiency. When the design variables that yield the highest system efficiency are combined, the resulting overall efficiency and heat recovery rate are 45.11% and 68.58%, respectively. This study presents an integrated thermodynamic evaluation of an ammonia-fueled gas turbine combined with an SCO_2 power cycle, which has received limited attention in previous studies.

Keywords: Ammonia, Gas turbine, Supercritical CO_2 power cycle, Waste heat recovery, Thermodynamic analysis

Nomenclature

C	: Compressor
CO_2	: Carbon dioxide
C_P	: Specific heat at constant pressure
exh	: Exhaust gas
GT	: Gas turbine
H	: Energy rate
H_2O	: Steam
HHV	: High heating value
HRR	: Heat recovery rate
HX	: Heat exchanger
$\dot{m}$	: Mass flow rate
net	: Net
NH_3	: Ammonia
O_2	: Oxygen
$\dot{Q}$	: Heat transfer rate
ref	: Reference state
SCO_2	: Supercritical carbon dioxide
sys	: System
T	: Turbine, Temperature
$\dot{W}$	: Power
η	: Efficiency

1. Introduction

Owing to stricter environmental regulations pertaining to ship exhaust emissions imposed by the International Maritime Organization, the shipbuilding and shipping industries are accelerating the development of propulsion systems based on low-carbon alternative fuels **[1]-[3]**. Among various low-flashpoint fuels, ammonia has garnered considerable attention as a carbon-free fuel owing to its low boiling point of -33.4 ℃ at atmospheric

† Corresponding Author (ORCID: https://orcid.org/0000-0002-9662-2175): Professor, Division of Marine System Engineering, Korea Maritime & Ocean University, 727, Taejong-ro, Yeongdo-gu, Busan 49112, Korea, E-mail: kimyt@kmou.ac.kr, Tel: +82-51-410-4258

1 Assistant professor, Division of Marine System Engineering, Korea Maritime & Ocean University, E-mail: jskim87@kmou.ac.kr, Tel: +82-51-410-4266

2 Associate professor, Division of Marine System Engineering, Korea Maritime & Ocean University, E-mail: doyeop@kmou.ac.kr, Tel: +82-51-410-4282

pressure, which renders it relatively easy to store and transport, and its zero carbon dioxide (CO_2) emission during combustion **[4][5]**. Consequently, interest in the development and commercialization of ammonia-fueled ships has increased rapidly.

Recently, Hanwha Ocean has developed a marine gas turbine propulsion system fueled by ammonia in collaboration with Baker Hughes in the United States **[6]**. Compared with reciprocating internal combustion engines, gas turbines are smaller and lighter for the same power output and are advantageous in terms of start-up, shutdown, and maintenance **[7]**. Additionally, they are highly compatible with electric propulsion systems, thus rendering them a key component for integration with eco-friendly ship propulsion technologies **[8]**.

An inherent feature of gas turbines is the continuous release of hot exhaust gases, which enables the generation of additional power by recovering waste heat **[9]**. The supercritical carbon dioxide (SCO_2) power cycle has emerged as a next-generation option for the effective use of medium- to high-temperature waste heat and has received considerable attention in recent years **[10]**. Owing to its high thermodynamic efficiency, compact configuration, and adaptability to different heat sources, the SCO_2 power cycle is considered a strong candidate for replacing the conventional steam Rankine cycle in waste heat recovery systems **[11]**. The temperature of the gas turbine exhaust fulfills the heat source requirements of the SCO_2 power cycle, which renders the cycle particularly suitable for designing high-efficiency waste heat recovery systems **[12]**.

Major studies pertaining to SCO_2 power cycles for gas turbine waste heat recovery are as follows: Kim *et al.* **[13]** compared various cycle configurations and confirmed that the split cycle effectively minimized exergy loss and improved thermal efficiency. Hou *et al.* **[14]** suggested that a system combining SCO_2 recompression and regenerative cycles is advantageous for improving the part-load performance of ships. Li *et al.* **[15]** compared different SCO_2 power cycles for gas turbine waste heat recovery and concluded that dual heated cascade cycle-II is suitable for achieving maximum efficiency, whereas a partial heating cycle is recommended for a balanced overall performance. Li *et al.* **[16]** designed a partial-heating SCO_2 power cycle using gas turbine waste heat through multi-objective optimization from both thermodynamic and economic perspectives. Off-design analyses indicated that adjusting the maximum pressure of the cycle effectively accommodated changes in the exhaust gas conditions, whereas adjusting the minimum pressure effectively accommodated ambient-temperature variations. Park **[17]** analyzed the effects of SCO_2 impurity composition on cycle performance using a 500 kW SCO_2 Brayton cycle demonstration system for LM500 gas turbine waste heat recovery and reported that a decrease in SCO_2 purity reduced both efficiency and the power output.

Although many studies have examined SCO_2 power cycles for general gas turbine waste heat recovery **[13]-[17]**, they primarily focused on conventional gas turbines and did not consider the unique exhaust characteristics of ammonia combustion. Meanwhile, previous studies pertaining to ammonia-based systems investigated the fuel supply, thermochemical recuperation, and gas turbine performance **[6]**, whereas an integrated analysis combining an ammonia-fueled gas turbine with an SCO_2 power cycle has not been reported. To address this research gap, an ammonia-fueled marine gas turbine cycle and an SCO_2 power cycle utilizing turbine exhaust gas as the heat source were modeled. The thermodynamic performance was analyzed with respect to variations in the key design parameters. The findings are expected to serve as useful guidelines for the development of high-efficiency ammonia-fueled marine gas turbine systems integrated with the SCO_2 power cycle.

2. System Concept

Figure 1 shows schematic diagrams of the ammonia gas turbine cycle (a) and SCO_2 power cycle (b). The basic concept of each system is as follows:

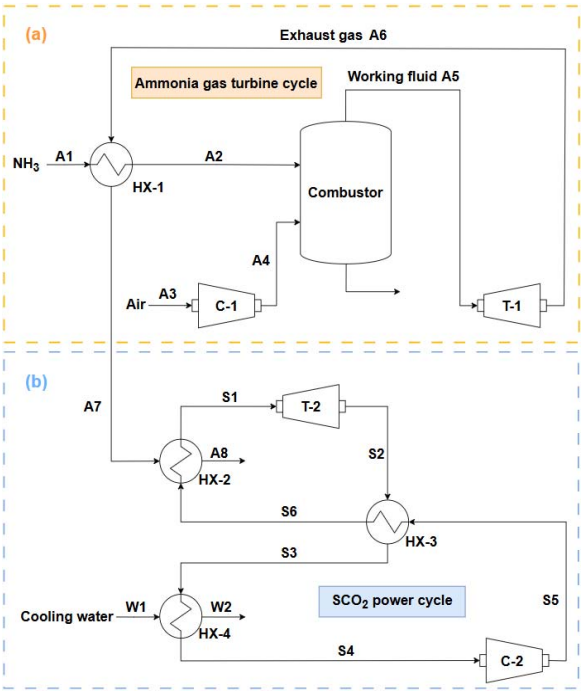

Figure 1: Schematic illustrations of ammonia gas turbine cycle (a) and supercritical CO_2 power cycle (b)

2.1 Ammonia Gas Turbine Cycle

Ammonia enters the system in state A1. In heat exchanger HX-1, ammonia is heated to state A2 by recovering waste heat from the exhaust gas (A6) discharged from the gas turbine (T-1). Meanwhile, ambient air enters the air compressor (C-1) in state A3 and is discharged in state A4. Subsequently, ammonia and air are supplied to the combustor, where they undergo a chemical reaction and combustion, as described in **Equation (1) [18]**.

$$4NH_3 + 3O_2 \rightarrow 2N_2 + 6H_2O \quad (1)$$

The combusted working fluid (A5) causes the gas turbine (T-1) to generate power, and the exhaust gas (A6) flows to HX-1 to heat the ammonia fuel, which is then released in state A7. The exhaust gas (A7) departing HX-1 enters the heater (HX-2) of the SCO_2 power cycle and serves as the heat source for heating CO_2.

2.2 SCO_2 Power Cycle

The SCO_2 power cycle is located below the ammonia gas turbine cycle, and its T–s diagram is presented in **Figure 2**. CO_2 exhibits the critical state at 7.38 MPa and 30.98 °C **[10]**. The diagram shows that the SCO_2 power cycle operates in the supercritical region above this critical point. The exhaust gas (A7) entering the heater (HX-2) heats CO_2 and is then discharged in state A8. The heated CO_2 (S1) expands to state S2 in the turbine (T-2) to generate power. In this study, an intermediate heat exchanger (IHX, HX-3) was considered to improve the cycle efficiency. The CO_2 in state S2 is first cooled to S3 via heat exchange with CO_2 in state S5 in HX-3. Subsequently, it is further cooled to S4 through heat exchange with cooling water in the cooler (HX-4). The CO_2 in state S4 is compressed to S5 by the compressor (C-2) and then heated to S6 in HX-3. Finally, CO_2 returns to HX-2, thus completing the cycle.

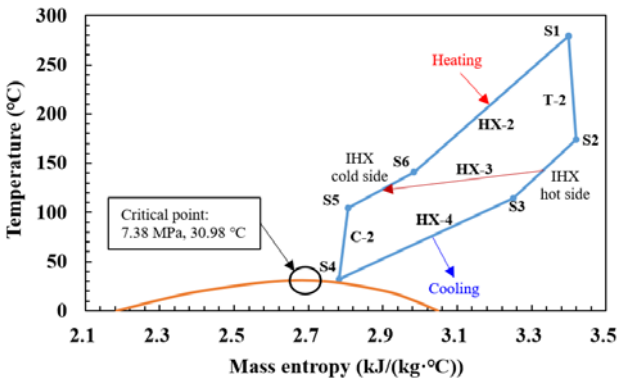

Figure 2: T–s diagram of supercritical CO_2 power cycle

3. System Modeling and Analysis Method

In this study, the system was modeled and analyzed under steady-state conditions using the commercial process-simulation software Aspen HYSYS V12.1 **[19]**. The real gas equation used was the Peng–Robinson equation of state **[20][21]**. Pressure drops and heat losses within the system were disregarded. This assumption affects the absolute values but not the overall trends discussed in this study.

3.1 Ammonia Gas-Turbine Cycle

The default modeling conditions of the ammonia gas turbine were obtained from a paper by Kim **[6]** and are summarized in **Table 1**.

Table 1: Default modeling conditions of ammonia gas turbine cycle

Item	Parameter	Unit	Value
A1	NH_3 inlet mass flow rate	kg/h	550
A1	NH_3 inlet temperature	℃	20
A1	NH_3 inlet pressure	bar	15
A3	Air inlet temperature	℃	20
A3	Air inlet pressure	atm	1
A5	Gas turbine inlet temperature	℃	1100
A6	Gas turbine outlet pressure	atm	1
C-1	Air compressor efficiency	%	85
T-1	Gas turbine efficiency	%	90

Table 2: Default modeling conditions of supercritical CO_2 power cycle

Item	Parameter	Unit	Value
S1	CO_2 turbine inlet pressure	bar	220
S4	CO_2 compressor inlet temperature	℃	32
S4	CO_2 compressor inlet pressure	bar	74
W1	Cooling water inlet mass flow rate	kg/h	90000
W1	Cooling water inlet temperature	℃	20
W1	Cooling water inlet pressure	bar	2
W2	Cooling water outlet temperature	℃	27
C-2	CO_2 compressor efficiency	%	80
T-2	CO_2 turbine efficiency	%	90

Table 3: Value ranges of key design variables for thermodynamic analysis

Item	Parameter	Unit	Value
A1	NH_3 inlet pressure	bar	9~21
A5	Gas turbine inlet temperature	℃	900~1300
S1	CO_2 turbine inlet pressure	bar	200~240
HX-2	Minimum approach temperature	℃	10~30
W2	Cooling water outlet temperature	℃	25~29

Referring to the study by Pashchenko *et al.* **[20]**, the temperature of the ammonia (A2) heated in HX-1 was assumed to be 50 °C lower than that of the exhaust gas (A6) discharged from the gas turbine. Based on a previous study **[6]**, the pressure of the air (A4) discharged from the air compressor was set to be equal to the pressure of the supplied ammonia fuel (A1). The airflow supplied to the compressor (A3) was controlled to satisfy the required turbine inlet temperature (A5).

3.2 SCO_2 Power Cycle

The default modeling conditions of the SCO_2 power cycle were obtained from a paper by Hou *et al.* [14] and are summarized in **Table 2**. Here, the minimum approach temperature of the CO_2 heater (HX-2) for heat exchange between the gas turbine exhaust gas and CO_2 was set to 20 °C. Additionally, the minimum approach temperature of the IHX (HX-3) was set to 10 °C.

3.3 System analysis method

Table 3 lists the value ranges of the key design variables for the thermodynamic analysis. The ranges were selected by varying each design variable around the baseline modeling conditions, as summarized in **Tables 1** and **2**. Using these ranges, parametric analyses were performed under the default modeling conditions.

In this study, the thermodynamic performance was evaluated based on the net power output, system efficiency, and heat recovery rate, while exergy analysis was not considered. The net power output of the system was calculated using **Equations (2)-(4) [6]**. The total net power output ($\dot{W}_{net}$) was obtained by summing the net power outputs of the ammonia gas turbine cycle ($\dot{W}_{GT,net}$) and the SCO_2 power cycle ($\dot{W}_{SCO_2,net}$).

$$\dot{W}_{GT,net} = \dot{W}_{T-1} - \dot{W}_{C-1} \tag{2}$$

$$\dot{W}_{SCO_2,net} = \dot{W}_{T-2} - \dot{W}_{C-2} \tag{3}$$

$$\dot{W}_{net} = \dot{W}_{GT,net} + \dot{W}_{SCO_2,net} \tag{4}$$

The system efficiency (η_{sys}) can be expressed as shown in **Equation (5) [6]**. Specifically, it can be calculated using the ammonia mass flow rate $\left(\dot{m}_{NH_3}\right)$, higher heating value ($HHV_{NH_3}$), and system net power output ($\dot{W}_{net}$).

$$\eta_{sys} = \frac{\dot{W}_{net}}{\dot{m}_{NH_3} HHV_{NH_3}} \tag{5}$$

Equations (6) and **(7)** represent the heat-recovery rate (HRR) and energy rate of the exhaust gas (H_{exh}), respectively **[6]**. Here, $\sum \dot{Q}_{HX}$ denotes the sum of the heat transfer rates from HX-1 and HX-2, which recover the waste heat energy from the exhaust gas. The exhaust gas composition was obtained from the combustion reaction, and the software calculated the C_p and related properties using the Peng–Robinson equation of state.

$$HRR = \frac{\sum \dot{Q}_{HX}}{H_{exh}} \tag{6}$$

$$H_{exh} = \dot{m}_{exh} C_P \left(T_{exh} - T_{ref}\right) \tag{7}$$

4. Results and Discussion

4.1 Ammonia Inlet Pressure

Figure 3 presents the analysis results for various ammonia inlet pressures in the ammonia gas turbine cycle. As shown in **Figure 3(a)**, both the power output of T-1 and the power consumption of C-1 increased with pressure. An increase in the inlet pressure of ammonia increased the outlet pressure of the air compressor, thereby increasing the power consumption of C-1. Additionally, the air mass flow rate increased, as shown in **Figure 3(b)**. As the ammonia inlet pressure increased, the combustion process released more energy; thus, a higher air mass flow rate was required to maintain a constant gas turbine inlet temperature. The increase in both the pressure and air mass flow rate resulted into a higher power output for T-1. In **Figure 3(b)**, the exhaust gas temperature decreased with increasing ammonia inlet pressure. This is because, with the turbine outlet pressure fixed at atmospheric pressure, a higher pressure ratio results in a greater enthalpy drop. Consequently, the reduced exhaust gas temperature decreases the power output of T-2, as shown in **Figure 3(a)**.

Table 4 shows that the power generated by the gas turbine cycle increased with pressure, whereas that generated by the SCO_2 cycle decreased. The total net power output and system efficiency increased proportionally with the ammonia inlet pressure.

Figure 3(c) shows the exhaust gas energy and heat transfer rates of HX-1 and HX-2. Although all the values decreased with increasing ammonia inlet pressure, the decrease in the exhaust gas energy rate was greater than that in the heat transfer of HX-1 and HX-2, thus resulting in an increase in the HRR.

In general, varying the ammonia inlet pressure first changed the air mass flow rate and the work of the compressor and turbine. This altered the exhaust gas temperature and heat transfer characteristics of HX-1 and HX-2, thus resulting in the observed changes in the total net power, system efficiency, and HRR.

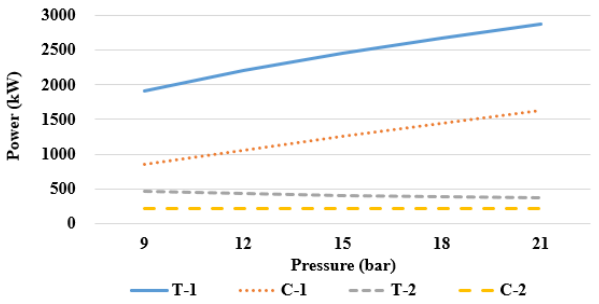

(a)

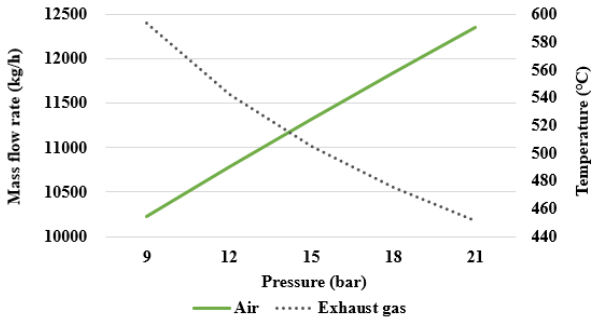

(b)

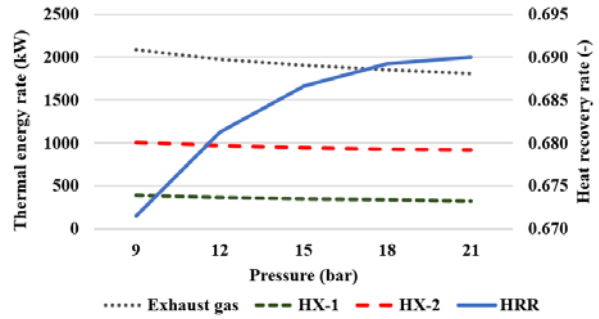

(c)

Figure 3: Analysis results based on ammonia inlet pressure

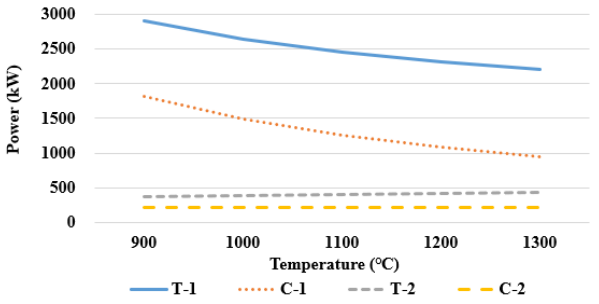

(a)

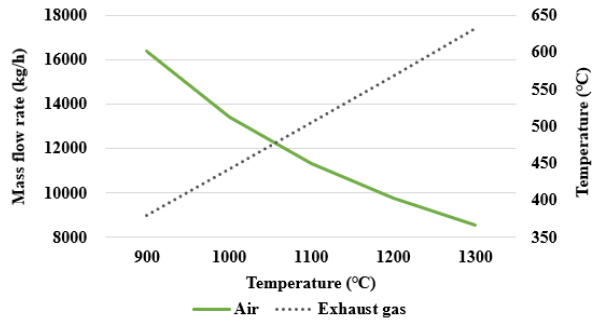

(b)

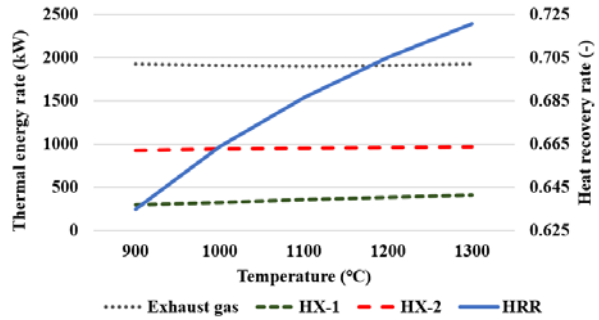

(c)

Figure 4: Analysis results based on gas turbine inlet temperature

Table 4: Key performance results based on ammonia inlet pressure

Pressure (bar)	$\dot{W}_{GT,net}$ (kW)	$\dot{W}_{SCO_2,net}$ (kW)	$\dot{W}_{net}$ (kW)	η_{sys} (-)
9	1066.9	254.1	1321.0	0.389
12	1142.8	221.0	1363.8	0.402
15	1191.4	197.1	1388.5	0.409
18	1223.8	179.1	1402.9	0.413
21	1245.6	165.0	1410.7	0.416

4.2 Gas Turbine Inlet Temperature

Figure 4 shows the analysis results for various gas turbine inlet temperatures in the ammonia gas turbine cycle. As shown in **Figure 4(a)**, the power output of T-1 and the power consumption of C-1 decreased with increasing temperature.

When the gas turbine inlet temperature increased, the required air mass flow rate decreased, as illustrated in **Figure 4(b)**. At a higher gas turbine inlet temperature, less air is required to reach the target combustion temperature, thus reducing the power consumption of C-1. Additionally, the reduced working fluid flow into the gas turbine decreases the power output of T-1. Based on **Figure 4(b)**, an increase in the gas turbine inlet temperature results in a higher exhaust gas temperature and a greater power output by T-2.

As shown in **Table 5**, the net output of the gas turbine cycle increased with the turbine inlet temperature. As the gas turbine inlet temperature increased, the decrease in the power consumption of C-1 exceeded the decrease in the power output by T-1, and the net power output of the SCO_2 power cycle also increased. Consequently, both the total net power output and system

Table 5: Key performance indicators for various gas turbine inlet temperatures

Temperature (°C)	$\dot{W}_{GT,net}$ (kW)	$\dot{W}_{SCO_2,net}$ (kW)	$\dot{W}_{net}$ (kW)	η_{sys} (-)
900	1092.3	168.2	1260.5	0.371
1000	1149.3	184.0	1333.3	0.393
1100	1191.4	197.1	1388.5	0.409
1200	1224.1	208.2	1432.3	0.422
1300	1250.9	217.4	1468.4	0.433

efficiency improved at higher gas turbine inlet temperatures.

Figure 4(c) shows the exhaust gas energy and heat transfer rates of HX-1 and HX-2. Although the exhaust gas energy rate remained almost unchanged as the gas turbine inlet temperature increased, the heat transfer rates of HX-1 and HX-2 increased. Consequently, HRR increased at higher inlet temperatures.

4.3 CO_2 Turbine Inlet Pressure

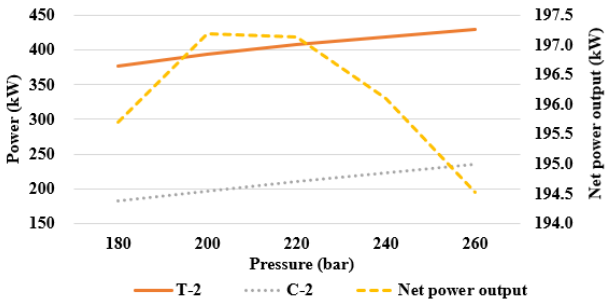

(a)

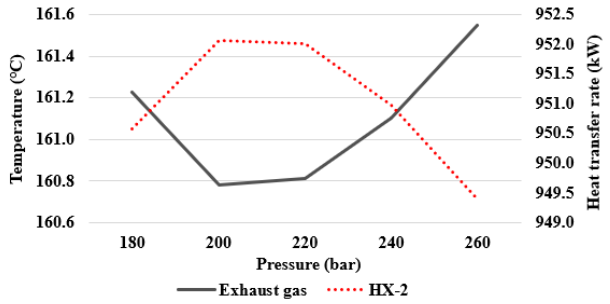

(b)

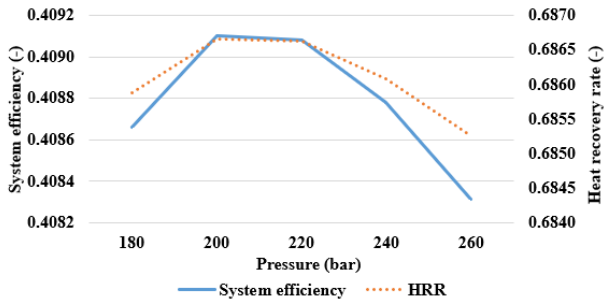

(c)

Figure 5: Analysis results based on CO_2 turbine inlet pressure

Figure 5 shows the analysis results for various CO_2 turbine inlet pressures during the CO_2 power cycle. As shown in **Figure 5(a)**, the power output of T-2 increased as the pressure ratio increased with the inlet pressure. Simultaneously, the power consumption of C-2 increased. However, the growth rates of T-2's power output and C-2's power consumption differed as the CO_2 inlet pressure increased. Based on the result, the SCO_2 power cycle achieved its maximum net power output of 200 bar. This indicates that, at approximately 200 bar, the effective enthalpy drop available for expansion in T-2 exceeded the enthalpy increase required for compression in C-2 by the largest margin.

Figure 5(b) shows that the exhaust gas temperature at A8 decreased with pressure up to 200 bar and then increased again, whereas the heat transfer rate of HX-2 increased to its peak at 200 bar before decreasing at higher pressures. As shown in **Figure 5(c)**, both the system efficiency and HRR reached their maximum values at 200 bar. This suggests that a turbine inlet pressure of approximately 200 bar provides the optimal operating conditions for the SCO_2 power cycle.

Based on these results, varying the CO_2 turbine inlet pressure changed the pressure ratio and the work of the turbine and compressor, thus altering the heat transfer rate of HX-2 and the exhaust gas temperature. These effects resulted in the observed maximum net power and system efficiency at approximately 200 bar.

4.4 Minimum Approach Temperature of HX-2

Figure 6 shows the analysis results obtained by varying the minimum approach temperature of HX-2 during the SCO_2 power cycle. In previous studies pertaining to SCO_2 power cycles using exhaust gas as the heat source, the minimum approach temperature between the exhaust gas and CO_2 in the heater was commonly fixed at 30 °C **[13][22]**. In the present study, this value was used as a reference, and the analysis range was extended by varying the HX-2 minimum approach temperature from 10 °C to 30 °C.

Figure 6(a) shows that the power output of T-2 decreased with increasing temperature. This is because, under a constant heat source inlet temperature, a higher minimum approach temperature reduces the CO_2 turbine inlet temperature. Meanwhile, the power consumption of C-2 remained almost unchanged. Therefore, the net power output of the SCO_2 power cycle decreased as the minimum approach temperature increased.

Figure 6(b) shows that an increase in the minimum approach temperature reduced the utilization of the exhaust gas waste heat

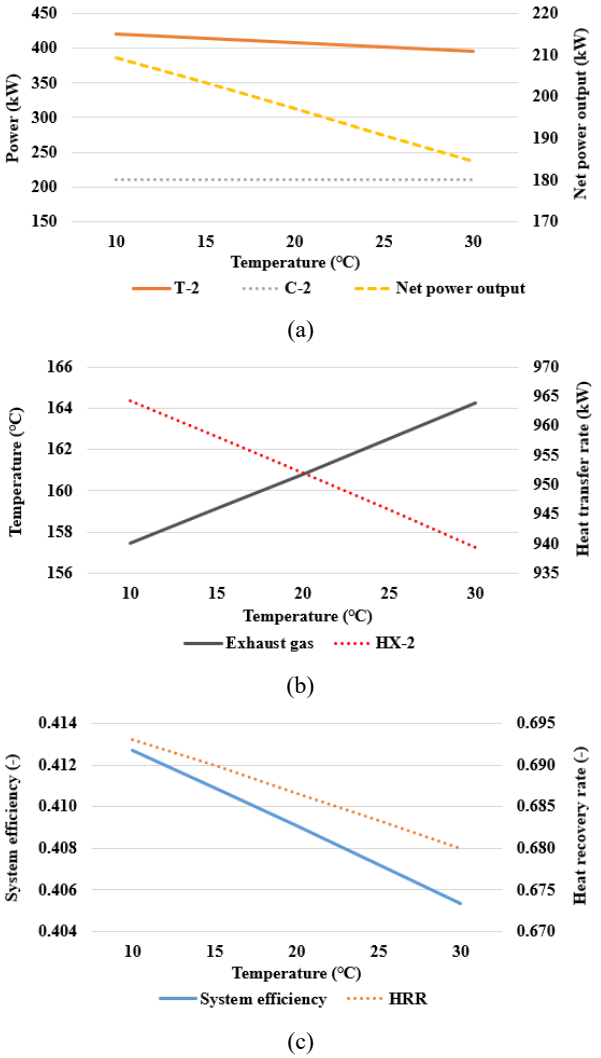

Figure 6: Analysis results based on minimum approach temperature of HX-2

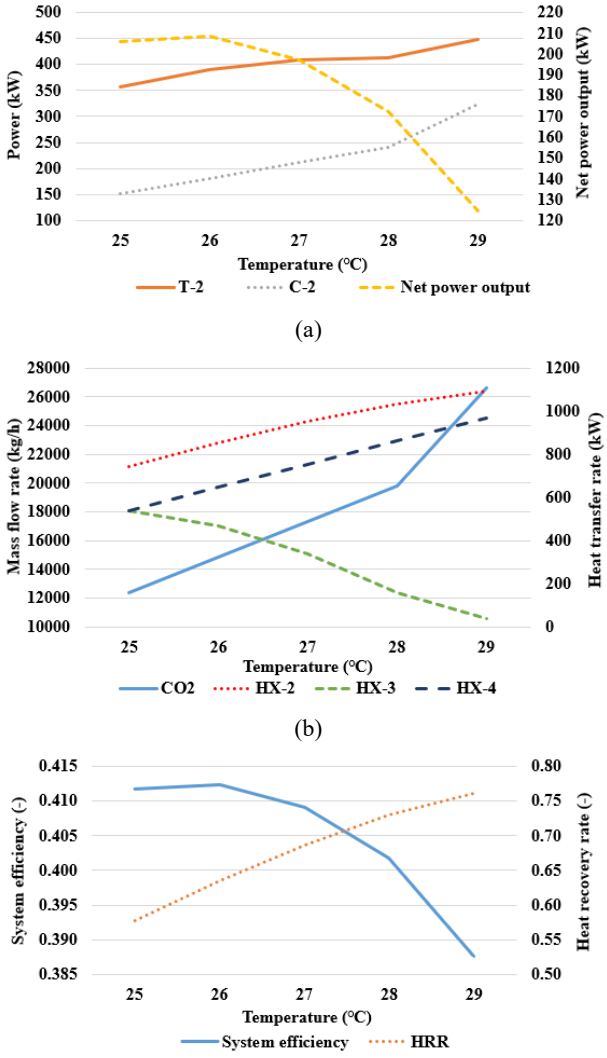

Figure 7: Analysis results based on cooling water outlet temperature

in HX-2, thereby increasing the exhaust gas temperature at A8 and decreasing the heat transfer rate of HX-2.

Thus, **Figure 6(c)** shows that both the overall system efficiency and HRR reached their maximum when the minimum approach temperature was at its lowest. At a lower minimum approach temperature, the CO_2 departing from HX-2 can reach a temperature closer to that of the exhaust gas, thus increasing the enthalpy drop available for expansion in T-2 and reducing the unused exhaust gas energy. This indicates that, in the SCO_2 power cycle, minimizing the minimum approach temperature of the heat exchanger serving as the heater is advantageous for both the system performance and heat recovery.

4.5 Cooling Water Outlet Temperature

Figure 7 shows the results obtained by varying the cooling water outlet temperature of the CO_2 cooler during the SCO_2 power cycle. **Figure 7(a)** shows the variations in T-2's power output and C-2's power consumption with respect to the cooling water outlet temperature. Both values increased with the outlet temperature, and the net power output of the SCO_2 power cycle reached its maximum at 26 °C.

As shown in **Figure 7(b)**, the heat transfer rate of HX-4 increased with the cooling water outlet temperature, thus resulting in a higher CO_2 mass flow rate in the cycle. This higher mass flow rate enhanced the power output of T-2 and the power consumption of C-2. However, the increased flow reduced the heat transfer capability of HX-3 because the gas passed through without sufficient thermal exchange. Consequently, the CO_2 departing from HX-3 (S6) entered HX-2 at a relatively low temperature, and HX-2 must provide additional heat transfer to satisfy the required turbine inlet condition.

Table 6: Values of key design variables yielding maximum efficiency

Item	Parameter	Unit	Value
A1	NH_3 inlet pressure	bar	21
A5	Gas turbine inlet temperature	℃	1300
S1	CO_2 turbine inlet pressure	bar	200
HX-2	Minimum approach temperature	℃	10
W2	Cooling water outlet temperature	℃	26

As shown in **Figure 7(c)**, the overall system efficiency reached its maximum at 26 ℃, where the net power output of the SCO_2 power cycle was at its maximum as well. This implies that a cooling water outlet temperature of approximately 26 ℃ provides an appropriate balance among the increased CO_2 mass flow rate, the power output of T-2, the power consumption of C-2, and the internal heat transfer within the cycle. Additionally, it indicates that the cooling water outlet temperature must be controlled appropriately to achieve the maximum system efficiency. Meanwhile, the HRR reached its peak under the maximum heat transfer rate of HX-2.

These observations indicate that the cooling water outlet temperature controls the CO_2 mass flow rate and the heat transfer characteristics of HX-2, HX-3, and HX-4, which consequently affect the power output of T-2 and the power consumption of C-2, thus resulting in the maximum net power and system efficiency at approximately 26 °C.

4.6 Key Design Variables with Maximum Efficiency

Table 6 lists the values of key design variables that yielded the highest efficiency within the thermodynamic analysis range of this study. In the ammonia gas turbine cycle, higher ammonia inlet pressure and gas turbine inlet temperature resulted in a higher system efficiency. In the SCO_2 power cycle, a lower minimum approach temperature of HX-2 was advantageous. Additionally, the CO_2 turbine inlet pressure and the cooling water outlet temperature should be set to the appropriate values.

Using the variable values listed in **Table 6**, the system analysis results show that the overall system efficiency and HRR were 45.11% and 68.58%, respectively. These values can be improved through optimization by defining an objective function and adjusting the variables simultaneously.

5. Conclusion

In this study, an ammonia-fueled marine gas turbine cycle was modeled simultaneously with an SCO_2 power cycle that used the gas turbine exhaust as a heat source. Thermodynamic analysis was performed to evaluate the effects of varying the key design variables, and the main results are summarized as follows:

1) Higher ammonia inlet pressures and gas turbine inlet temperatures resulted in higher system efficiencies and HRRs.
2) A lower minimum approach temperature of HX-2 was advantageous for improving the system efficiency and HRR.
3) The appropriate CO_2 turbine inlet pressure yielded the highest system efficiency and HRR.
4) For maximum system efficiency, the appropriate cooling water outlet temperature should be adopted; however, the HRR increased with the cooling water outlet temperature.
5) Using the key design variables that yielded the maximum system efficiency, the resulting system efficiency and HRR were 45.11% and 68.58%, respectively.

Future studies may include system optimization, economic and environmental assessments, off-design performance evaluations under varying engine loads, and investigations into integration strategies with other shipboard systems. Additionally, the simplified steady-state model used in this study, which does not consider pressure drops, heat losses, and detailed component efficiencies, should be refined to reduce modeling uncertainty.
The thermodynamic characteristics identified in this study support the preliminary design and integration of SCO_2-based waste heat recovery into ammonia-fueled marine gas turbine propulsion and provide reference data for the further development of related systems.

Acknowledgement

This work was supported by the Korea Maritime & Ocean University Research Fund in 2025.

Author Contributions

Conceptualization, J.-S. Kim; Methodology, J.-S. Kim; Software, J.-S. Kim; Validation, J.-S. Kim and D.-Y. Kim; Formal Analysis, J.-S. Kim; Investigation, J.-S. Kim; Resources, J.-S. Kim; Data Curation, J.-S. Kim; Writing—Original Draft Preparation, J.-S. Kim; Writing—Review & Editing, D.-Y. Kim and Y.-T. Kim; Visualization, J.-S. Kim; Supervision, Y.-T. Kim; Project Administration, Y.-T. Kim; Funding Acquisition, Y.-T. Kim.

References

[1] J. -S. Kim and D. -Y. Kim, “Thermodynamic and economic analysis of cargo boil-off gas re-liquefaction systems for

ammonia-fueled LCO2 carriers," Journal of Marine Science and Engineering, vol. 12, no. 9, pp. 1642, 2024.

[2] J. -S. Kim and D. -Y. Kim, "Energy, exergy, and economic (3E) analysis of SOFC-GT-ORC hybrid systems for ammonia-fueled ships," Journal of Marine Science and Engineering, vol. 11, no. 11, pp. 2126, 2023.

[3] J. -S. Kim and D. -Y. Kim, "Energy, exergy, and economic (3E) analysis of boil-off gas re-liquefaction systems using LNG cold energy for LNG-fueled ships," Journal of Marine Science and Engineering, vol. 11, no. 3, p. 587, 2023.

[4] S. -K. Jeong, Y. -T. Kim, and J. -S. Kim, "Simulation and analysis of a fuel supply system with vent control system for ammonia fueled ships," Journal of Advanced Marine Engineering and Technology, vol. 48, no. 5, pp. 260-267, 2024.

[5] S. -K. Jeong, J. -S. Kim, and Y. -T. Kim, "Optimization study of BOG re-liquefaction process for ammonia fueled ship," Journal of Advanced Marine Engineering and Technology, vol. 48, no. 4, pp. 167-176, 2024.

[6] J. -S. Kim, "Performance analysis of ammonia gas turbines with thermochemical recuperation and organic Rankine cycle application," Transactions of the Korean Society of Mechanical Engineers B, vol. 49, no. 7, pp. 411-420, 2025.

[7] A. I. Sayma, "Gas turbines for marine applications," Encyclopedia of Maritime and Offshore Engineering, pp. 1-10, 2017.

[8] D. Barsi, L. Frezza, F. Satta, Y. Luan, and P. Zunino, "Marine applications and design of high-efficiency small-scale gas turbines," Designs, vol. 8, no. 4, p. 66, 2024.

[9] D. Bonalumi, A. Giuffrida, and F. Sicali, "A case study of cascade supercritical CO2 power cycle for waste heat recovery from a small gas turbine," Energy Conversion and Management: X, vol. 14, pp. 100212, 2022.

[10] G. Manente and A. Lazzaretto, "Innovative biomass to power conversion systems based on cascaded supercritical CO2 Brayton cycles," Biomass and Bioenergy, vol. 69, pp. 155-168, 2014.

[11] L. Liu, Q. Yang, and G. Cui, "Supercritical carbon dioxide (s-CO2) power cycle for waste heat recovery: A review from thermodynamic perspective," Processes, vol. 8, no. 11, pp. 1461, 2020.

[12] M. Marchionni, G. Bianchi, and S. A. Tassou, "Review of supercritical carbon dioxide (sCO2) technologies for high-grade waste heat to power conversion," SN Applied Sciences, vol. 2, pp. 611, 2020.

[13] Y. M. Kim, J. L. Sohn, and E. S. Yoon, "Supercritical CO2 Rankine cycles for waste heat recovery from gas turbine," Energy, vol. 118, pp. 893-905, 2017.

[14] S. Hou, Y. Wu, Y. Zhou, and L. Yu, "Performance analysis of the combined supercritical CO2 recompression and regenerative cycle used in waste heat recovery of marine gas turbine," Energy Conversion and Management, vol. 151, pp. 73-85, 2017.

[15] B. Li, S. Wang, K. Wang, and L. Song, "Comparative investigation on the supercritical carbon dioxide power cycle for waste heat recovery of gas turbine," Energy Conversion and Management, vol. 228, pp. 113670, 2021.

[16] B. Li, S. Wang, Y. Xu, and L. Song, "Study on the off-design performance of supercritical carbon dioxide power cycle for waste heat recovery of gas turbine," Energy Conversion and Management, vol. 233, pp. 113890, 2021.

[17] J. H. Park, "Thermodynamic analysis of supercritical CO2 power generation system for waste heat recovery with impurities in CO2," Applied Thermal Engineering, vol. 258, pp. 124540, 2025.

[18] T. Fujimori and T. Suda, "Ammonia energy value chain for carbon neutrality from production to utilization," IHI Engineering Review, vol. 55, no. 1, pp. 1-5, 2022.

[19] Aspen Technology Inc., Aspen HYSYS V12.1 User Guide, Bedford, MA, USA, 2021.

[20] D. Pashchenko, R. Mustafin, and I. Karpilov, "Ammonia-fired chemically recuperated gas turbine: Thermodynamic analysis of cycle and recuperation system," Energy, vol. 252, pp. 124081, 2022.

[21] M. E. Siddiqui and K. H. Almitani, "Proposal and thermodynamic assessment of S-CO_2 Brayton cycle layout for improved heat recovery," Entropy, vol. 22, no. 3, pp. 305, 2020.

[22] Y. M. Kim, Y. D. Lee, and K. Y. Ahn, "Parametric study of a supercritical CO2 power cycle for waste heat recovery with variation in cold temperature and heat source temperature," Energies, vol. 14, no. 20, pp. 6648, 2021.